

Kinematics of the local disc from the RAVE survey and the Gaia first data release

Annie C. Robin¹, Olivier Bienaymé², José G. Fernández-Trincado¹, and Céline Reylé

¹ Institut Utinam, CNRS UMR6213, Univ. Bourgogne Franche-Comté, OSU THETA, Observatoire de Besançon, BP 1615, 25010 Besançon Cedex, France

e-mail: annie.robin@obs-besancon.fr

² Observatoire Astronomique de Strasbourg, Université de Strasbourg, CNRS, 11 rue de l'Université, F-67000 Strasbourg, France

Abstract

Aims. We attempt to constrain the kinematics of the thin and thick discs using the Besançon population synthesis model together with RAVE DR4 and Gaia first data release (TGAS).

Methods. The RAVE fields were simulated applying a detailed target selection function and the kinematics was computed using velocity ellipsoids depending on age in order to study the secular evolution. We accounted for the asymmetric drift computed from fitting a Stäckel potential to orbits. Model parameters such as velocity dispersions, mean motions, velocity gradients, were adjusted using a ABC-MCMC method. We made use of the metallicity to enhanced the separation between thin and thick discs.

Results. We show that this model is able to reproduce the kinematics of the local discs in great detail. The disc follows the expected secular evolution, in very good agreement with previous studies of the thin disc. The new asymmetric drift formula, fitted to the Stäckel potential described in Bienaymé et al (2015), fairly well reproduces the velocity distribution in a wide solar neighbourhood. The U and W components of the Solar motion determined with this method agree well with previous studies. However we find a smaller V component than previously thought, essentially due to the inclusion of the variation of the asymmetric drift with distance to the plane. The thick disc is represented by a long period of formation (at least 2 Gyr) during which it is shown that the mean velocity increases with time, while the scale height and scale length decrease, very consistently with a collapse phase with conservation of angular momentum.

Conclusions. This new Galactic dynamical model is able to reproduce the observed velocities in a wide solar neighborhood at the level of quality of the TGAS-RAVE sample, allowing to constrain the thin and thick disc dynamical evolution, as well as determining the Solar motion.

Key words. Galaxy:evolution, Galaxy:dynamics, Galaxy:disk, Galaxy:kinematics, Galaxy: formation, Galaxy: stellar content

1. Introduction

Kinematics of the local disc is a popular subject of debate since several decades. Several issues have been considered, such as: how to disentangle the Solar motion from the local standard of rest; how fast is the secular evolution; does the thin disc separates from the thick disc in velocity space; what is the importance of the dark matter halo locally and its imprint on the stellar kinematics; where does the vertex deviation come from and how it relates to the spiral structure; what is the effect of resonances of the bar and spiral arms locally; what was the effect of the radial migration of the populations over times.

Recent large scale spectroscopic surveys are now giving the opportunity to better understand those problems. Numerous direct analysis of such surveys (GCS (Nordström et al. 2004), RAVE (Kordopatis et al. 2013; Kunder et al. 2017), APOGEE (Eisenstein et al. 2011), Gaia-ESO (Randich et al. 2013), among the largest one) are giving outstanding contributions to these studies, thanks to the large statistics possible with several hundred thousands of measurements homogeneous on the sky, in opposition to earlier studies dealing with samples of a few hundred stars at most.

Inverse methods have been used to deduce the Solar motion, secular evolution, based on estimations of distances to stars (generally photometric distances, sometime spectrophotometric

distances, rarely parallaxes). They also use age estimations in order to deduce the secular evolution of the stellar populations. However these estimates (ages, distances) are generally strongly biased because the errors on ages and distances have strongly dissymmetric distributions, far from Gaussian. Moreover, the sample selection functions also introduce their own bias.

We here consider a complementary approach to analyse the kinematics of a local sample using the population synthesis approach (Crézé & Robin 1983). The method allows to simulate the survey selection function and to avoid the use of photometric distances and ages by using instead the distribution of stars in the space of observables. The method is based on simple realistic assumptions for different populations and constrained by the Boltzmann equation (Bienaymé et al. 1987).

The method makes use of the latest version of the Besançon Galaxy Model, hereafter BGM (Robin et al. 2014; Czekaj et al. 2014) and is applied on the RAVE survey (DR4, Kordopatis et al. (2013)) and proper motions from TGAS part of the Gaia DR1 (Gaia Collaboration et al. 2016) in order to constrain the kinematics of the different populations. We apply an ABC-MCMC (Approximate Bayesian Computation Markov Chain Monte Carlo, Marin et al. (2011)) scheme to adjust the model parameters in the space of observables of the survey data.

Section 2 describes the data sets and the selections applied on both the data and the simulations. The kinematical model parameters of the thin and thick discs are given in section 3. The

Send offprint requests to: A.C. Robin

ABC-MCMC method is described in section 4, while the results are reported and discussed in section 5. Section 6 summarizes the main conclusions drawn from this study.

2. Data set and selection function

2.1. Sample selection

We make use of the RAVE data release DR4 (Kordopatis et al. 2013) which contains radial velocities, astrophysics parameters and abundances for more than 400,000 stars in a wide solar neighbourhood (up to 2 kpc from the Sun). It also contains proper motions for a large number of these stars. However since the publication of the TGAS catalogue of proper motions coming from the Gaia mission first release, we used instead these space based proper motions which are much more accurate and free from large systematics (Arenou et al. 2017). The accuracy of the radial velocities is of the order of 2 km/s while the proper motions are better than 1 mas/yr. These data set provides very accurate informations on the 3D velocities of stars.

The RAVE survey covers nearly all the southern hemisphere, although in each field only a subset of available stars are measured, randomly selected in order to have an unbiased sample. The stars are selected in bins of apparent I magnitude well representing all type of stars in each magnitude bin. We have limited the analysis in the range $9 < I < 12$ where the astrophysical parameters are accurate enough. Not all stars with velocities have measured metallicities. In particular at $I > 11.5$ the proportion of stars with reliable metallicities drops to about 40%, while it is about 60% at brighter magnitudes. In order to use the metallicities and effective temperatures for distinguishing better the populations, we have used the RAVE sample of stars having metallicities $[M/H]_K$ available and temperatures between 3800 K and 8000 K. We also avoided using low latitude fields ($|b| < 25^\circ$) because these regions have a complex target selection due to extinction, more difficult to reproduce correctly in the simulated sample, which limits the sample to 294,206 stars.

At the time of the submission of this publication, the RAVE DR5 was recently available with a preliminary version of the associated paper accessible on archiv.org, but that version was not yet accepted. For this reason, we maintained our analysis based on the RAVE DR4 data. Also, our model-observations comparison is based, for a half, on proper-motion and magnitudes, non RAVE data, while most RAVE radial velocities remain identical from DR4 to DR5. In future works, we will base analysis of the Galactic properties using the BGM and the DR5 since it presents significant improvements such as 30,000 new stars included, more accurate $[M/H]$ and T_{eff} with bias corrected for the extreme values of $[M/H]$ and T_{eff} .

We can estimate the impact of having used the DR4 instead of the DR5 release for the present analysis. DR5 data are improved thanks to a recalibration of the temperature, gravity and metallicity. Figures 4, 5 and 6 (Kunder et al. 2017) allow to compare the mean DR5 versus DR4 values. The difference is not negligible in gravity but we are not using it in the present study. The definition of our subsamples for analysis of observed proper motions and radial velocities is based on cuts in I magnitudes (same magnitudes from DR4 to DR5), cut in temperature at 5300 K, and cuts in metallicity $[M/H]$, split at -1.2, -0.8, -0.4, and 0. Our $[M/H]$ and T_{eff} cut values are not modified with the new calibrations of Kunder et al. (2017). Hence, using instead the DR5 would not have introduced systematic changes of the content of our subsamples. Furthermore, the proper motions are

extracted from the TGAS catalogue, and radial velocities are not modified at the exception of some mismatch corrections.

TGAS proper motions are used for each star selected in the RAVE survey. It could have been possible to use the other TGAS stars, but at the expense of not having any information on metallicity and effective temperature, which are used here to separate thin and thick disc populations, and dwarfs from giants. Moreover we found that the TGAS sample cross-identified with RAVE drops in completeness below magnitude 10. Hence we limited the analysis at this magnitude for the proper motion histograms.

2.2. Simulations

The simulations are done using the revised version of BGM (Czekaj et al. 2014) where the thin disc population is modelled with a decreasing star formation rate, a revised IMF, new evolutionary tracks and atmosphere models, and including the simulation of binarity. For the thick disc and halo population, the simulations are based on Robin et al. (2014) where the thick disc structural and age parameters have been constrained together with the halo from color-magnitude diagrams fitting to SDSS and 2MASS photometry. We adopt here the thick disc model shape B (secant squared in z_{gal}) and a Hernquist halo with a core radius of 5.17 kpc and an axis ratio of 0.776. Haywood et al. (2013) proposed that the probable period of formation of the thick disc extended over 3-4 Gyr, from 9 to 13 Gyr. In Robin et al. (2014) we showed that a good description of the populations in the thick disc, to reproduce SDSS and 2MASS data, was obtained when it is simulated by an extended star formation period, which can be simplified in the sum of two episodes, one about 12 Gyr ago and the second one 10 Gyr ago. However there are no evidence of two separate episodes, but rather a continuity between these two isochrones. The best model was obtained when the thick disc older stars are located in a wider structure, and the younger stars in a smaller ones. Typically the scales in the older phase were estimated to be 2.9 kpc and 0.8 kpc, respectively for the scale length and the scale height, and in the younger phase they were estimated to 2.0 kpc and 0.33 kpc (assuming exponential radially and sech^2 vertically). Moreover the ratio in local density of these two phases was found to be 0.15. Hence the young thick disc is the dominant component while the old thick disc can be considered as marginal, although it is well detected in large surveys. It might coincide with the metal-weak thick disc identified a long time ago by Norris et al. (1985). On the point of view of the kinematics, if this scenario is correct, one should be able to estimate a difference in rotation between these two phases, i.e. the older wider phase should rotate more slowly than the younger phase.

We performed simulations in every RAVE field in the same photometric system and selected randomly the same number of stars as observed by RAVE in each I magnitude bin defined by RAVE, that is 9-9.5, 9.5-10, 10-10.5, 10.5-10.8, 10.8-11.3, 11.3-11.7 and 11.7-12.

Figure 1 shows the comparison of the I magnitude distribution of the selected samples in observations and simulations. The distribution in I in the simulation is close to the one of the real data. In order to check the distribution in astrophysical parameters of the whole sample, Figure 2 presents the histogram of the distribution in effective temperature, gravity of the simulated and observed sample.

In some cases the number of stars with reliable radial velocities and metallicities in RAVE data is of the order of 50

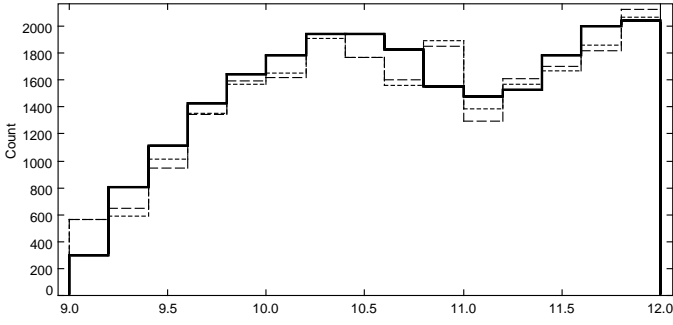


Figure 1. Distribution in I magnitude of the observed sample (solid line) of stars with reliable radial velocities and metallicities, and simulated sample (dashed and dotted line for two independent simulated samples) for the whole RAVE survey.

to 150 per field. It implies a significant Poisson noise when performing comparisons in metallicity bins. Therefore, we used simulations that have 5 times the number of observed stars to decrease the Poisson noise, and we performed 8 independent runs starting from random initial values in order to avoid to be stacked in local maxima of the likelihood.

3. Basis of the kinematical model

The kinematics of the stars is computed from simple assumptions of relations between ages and velocity ellipsoids for the thin disc, and *ad hoc* empirical values for the thick disc and the halo, as described below. The kinematics in the bar is more complex. In another study we are using the bar potential to derive the velocity distributions from test-particle simulations (Fernández-Trincado et al. in prep). For the purpose of the present work, the bar kinematics is not relevant since the bar population does not reach in significant number the RAVE sample. Although the bar potential can perturb the kinematics of the disc stars in the solar neighbourhood, we considered provisionally for this paper an axisymmetric potential locally. We adopted the usual reference system, with U towards the Galactic center, V towards rotation, and W towards the North Galactic Pole.

3.1. Thin disc

The thin disc kinematics is based on the velocity ellipsoids with dispersions varying with age, following Bienaymé et al. (1987) study. Table 1 gives the assumed age-velocity dispersion relation used in previous Besançon Galaxy Model (Robin et al. 2003) following Gómez et al. (1997) determination from Hipparcos sample. The velocity dispersions increase with age, as expected for a secular evolution from a circular disc. Holmberg et al. (2009) proposed velocity dispersions slightly higher than Gómez et al. (1997). RAVE and TGAS data give a good opportunity to derive a more accurate age-velocity dispersion relation. We here considered that the velocity dispersion increases with age following three different formulae: 1) a third order polynomial (Eq. 1); 2) the square root formula proposed by Wielen (1977) (Eq. 2); 3) the power law formula taken from Aumer et al. (2016) (Eq. 3).

$$\sigma_W = A + B \times \tau + C\tau^2 \quad (1)$$

Table 1. Velocity ellipsoid as a function of age for the thin disc seven components in the standard Besançon Galaxy Model

Subcomponent	Age range Gyr	σ_U km/s	σ_V km/s	σ_W km/s
1	0.-0.15	16.7	10.8	6.0
2	0.15- 1.	19.8	12.8	8.0
3	1.-2.	27.2	17.6	10.0
4	2.- 3.	30.2	19.5	13.2
5	3.- 5.	36.7	23.7	15.8
6	5.- 7.	43.1	27.8	17.4
7	7.-10.	43.1	27.8	17.5

$$\sigma_W = \sqrt{\alpha + \gamma \times \tau} \quad (2)$$

$$\sigma_W = k \times \tau^\beta \quad (3)$$

where τ is the age in Gyr.

Then the velocity dispersion in U and V are defined relatively to σ_W by the ratios σ_U/σ_V and σ_U/σ_W which are free parameters and assumed to be independent of time.

In the fitting process we also consider the vertex deviation, allowing for two different angles VD_a and VD_b , for stars of ages smaller or larger than 1 Gyr, respectively.

3.2. Thick disc

The thick disc velocity ellipsoid suffers from uncertainties mainly due to the way that this population is selected in different data sets. Indeed, the quite continuity (or lack of clear separation) of the two disc populations, when no elemental abundances are available, have been the source of misunderstanding and apparent inconsistency between various analyses. With the help of alpha element abundance ratio it can be easier to analyse, since it has been shown in local samples (Adibekyan et al. 2013) and more distant samples (Hayden et al. 2014), among others, that the thick disc better separates from the thin disc using $[\alpha/Fe]$ ratio. However, the abundances in RAVE DR4 are not accurate enough to distinguish clearly the thick disc from the thin disc sequence in the $[\alpha/Fe]$ versus $[Fe/H]$ plane. After several tests, we decided to use only $[Fe/H]$ for separating the populations in the present analysis.

From Robin et al. (2014) the scale length and scale height change from the beginning (12 Gyr ago) to the end of the phase (10 Gyr ago) due to contraction. Hence we expect that the velocity ellipsoid and rotation velocity will show similar behavior.

For the present analysis we have chosen to keep the velocity dispersions of the thick disc as free parameters as well as its rotation velocity, but we assumed that these parameters are different for the two thick disc episodes, mimicking a time evolution. The fourth order dependency on time of the velocity dispersion ellipsoids take this into account.

The other populations (halo, bar) are very marginal in RAVE survey and will not perturb the analysis.

3.3. Rotation curve and asymmetric drift

In order to simulate the kinematics of stars at larger distances from the Sun, we use the rotation curve produced by the mass model. To compute the radial force, we sum up the different

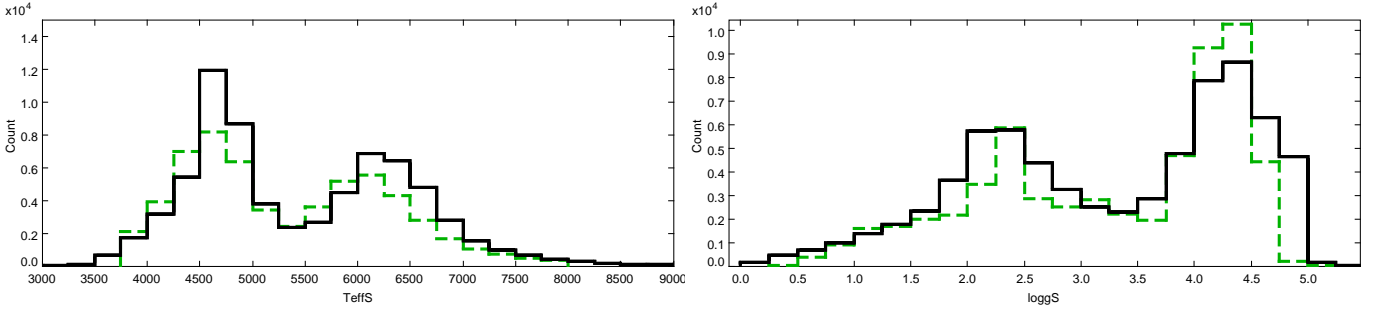


Figure 2. Distribution in effective temperature (left panel) and gravity (right panel) of the observed sample (solid line) of stars with reliable radial velocities and metallicities, and simulated sample (dashed line) for the selection $|b| > 20^\circ$ and $I < 12$.

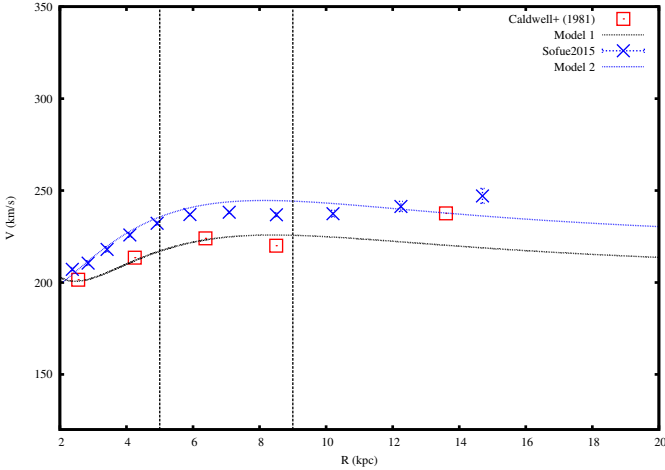


Figure 3. Rotation curve of the mass model, compared with Caldwell & Ostriker (1981) and Sofue (2015). The interval between the two dashed lines indicates the range of Galactocentric distances implied in the present study.

mass components (stellar populations, interstellar matter, dark matter halo) and derive the circular velocity as a function of Galactocentric radius. In this process described in Bienaymé et al. (1987) we used observational data, either from Caldwell & Ostriker (1981) or alternatively from Sofue (2015) to constrain the dark matter halo distribution and the thin disc ellipsoid axis ratio. The resulting rotation curves are presented in Figure 3. There is a significant difference between the two rotation curves, but at the Solar position their slopes are very similar. As we shall see below, they will result in a similar fit to RAVE+TGAS data because these data mainly constrain the velocity dispersions, the slope of the rotation curve and the asymmetric drifts but only put weak constraints on the amplitude of the rotation curve itself.

The asymmetric drift is then computed to take into account the change of circular velocity as a function of age and distance from the plane with regards to the rotation curve. It depends on the velocity dispersion ratio, on density and kinematic gradients and on the difference of radial force as a function of R_{gal} and z_{gal} .

In the past we used the simplified formula of the asymmetric drift proposed by Binney & Tremaine (2008) which is valid in the Galactic plane. In order to have a more consistent expression of the asymmetric drift as a function of distance from the plane, we make use of the gravitational potential inferred by the

mass distribution of the BGM. Bienaymé et al. (2015) proposed distribution functions based on a Stäckel approximation of the BGM potential, for which it is possible to compute a third integral of motion. An approximate fit of the variations of the asymmetric drift with $(R_{\text{gal}}, z_{\text{gal}})$ Galactocentric coordinates is computed and used in the kinematical modelling. This approximation is valid in the range $2 \text{ kpc} < R_{\text{gal}} < 16 \text{ kpc}$ and $-6 \text{ kpc} < z_{\text{gal}} < 6 \text{ kpc}$ and was shown to be a very good approximation, as the K_z is reproduced at better than 1%. The resulting rotational lag of different thin disc and thick disc subcomponents are shown to be very much depend on R_{gal} and z_{gal} . These dependencies are presented in Fig. 4.

3.4. Sun velocities

There have been a number of study trying to measure the peculiar velocities of the Sun. The U and W velocities are relatively well known and have been constrained at the level of 1-2 km/s. This is not the case for the V velocity which is uncertain due to difficulty to disentangle it from the mean circular motion of the LSR. Hence, while in the past it was admitted to be about 5-6 km/s (see i.e. Dehnen & Binney (1998) among others), more recent studies found much larger values. For example, Schönrich et al. (2010) found about 12 km/s from a subset of the Geneva-Copenhagen Survey (GCS), while Bovy et al. (2012) from APOGEE first data release (Ahn et al. 2014) found an even larger value of 26 ± 3 km/s). These values are not independent on the tracer selection, mostly K giants in the case of Bovy et al. (2012) and mostly dwarfs in the case of Schönrich et al. (2010). They also significantly depend on the rotation curve assumed, as well as on the distance between the Sun and the Galactic center. This is why in our analysis the Solar motion is a free parameter that can be influenced by other parameters, and by the way the asymmetric drift is modelled.

4. Setting up the MCMC

This study use a ABC-MCMC code based on a Metropolis-Hasting sampling, as described in Robin et al. (2014). Table 2 shows the set of model parameters to fit and their respective range. To estimate the goodness-of-fit for each model we compared directly histograms of radial velocity and proper motions between the model and the data. The bin steps in radial velocity and proper motions are 5 km/s and 5 mas/yr, respectively. But to improve the sensitivity of the analysis we separated stars using their metallicity and their temperature. The metallicity rather than α abundances was used because the accuracy in α in the RAVE survey does not allow to separate

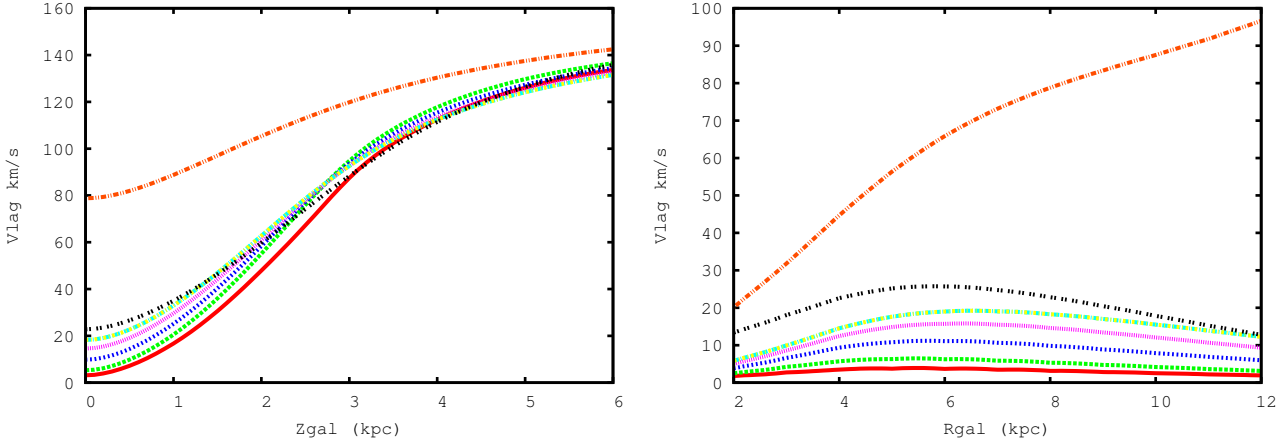


Figure 4. Asymmetric drift computed from the Stäckel approximation of the BGM for subcomponents 2 to 7 (thin disc, with ages increasing in solid red, long-dashed green, short-dashed blue, dotted magenta, dashed yellow-cyan), and for the young (dotted-dashed black) and old (dotted-dotted-dashed red) thick discs. Left panel: as a function of R_{gal} for $z_{\text{gal}} = 0$; Right panel: as a function of z_{gal} for $R = R_{\odot}$.

well the thin disc from the thick disc sequences, and we expect that the metallicity is more accurate. Moreover, to separate the young thick disc from the old thick disc, the metallicity is more efficient than the α abundances, as well to separate the metal rich thin disc from the normal thin disc.

We made use of 4 metallicity bins, where lower metallicities are dominated by the thick disc and higher metallicities by the thin disc. The minimum metallicity is -1.2 and the width of each bin is 0.4 dex. To separate dwarfs from giants, we cut in temperature at 5300 K, considering that cooler stars are mainly giants, while hotter ones are mainly dwarfs. However we do not explicitly assume that they are dwarfs or giants in the analysis. We just consider these 2 bins and compute histograms of velocities and likelihood for these 2 bins separately, in both data and simulations, to enhanced the efficiency of the fit of the parameters depending on ages. For the proper motions we use projections on Galactic coordinates, $\mu_l^* = \cos(b) \times \mu_l$ and μ_b , but for the South Galactic cap it is more interesting to project the proper motions parallel to the U and V vectors, U pointing towards the Galactic center, and V towards rotation. It makes the interpretation of histogram comparisons easier, showing well the skewness of the V distribution due to the asymmetric drift.

The likelihoods were computed separately for 11 regions of the sky, corresponding to different latitudes and quadrants in longitudes. The likelihood is based on the formula given in Bienaymé et al. (1987) for a Poisson statistics. Then, to intercompare different models with a different number of free parameters, we compute the Bayesian Information Criterion (BIC) following Schwarz (1978) which penalizes models having more free parameters (Eq. 4).

$$BIC = -2. \times Lr + k \times \ln(n). \quad (4)$$

where Lr is the likelihood, k is the number of parameters, and n the number of observations used in the likelihood computation.

At the end of the process, we consider the last third of each Markov chain, containing 200,000 iterations each, for 8 independent runs of the MCMC and compute the mean and dispersion for each fitted parameter.

Table 2. Set of parameters and range used in ABC-MCMC process. Units are km/s for velocities and radian for the vertex deviation. Thin disc parameters A, B, C are the coefficients of formula describing the evolution of σ_W with time (see text). The vertex deviation is for ages younger (VD_a) and older (VD_b) than 1 Gyr, and the scale lengths are given in kpc. Velocities and velocity dispersions are all given in km/s.

Component	Parameter	min	max
<i>Solar motion</i>			
	U_{\odot}	0.	20.
	V_{\odot}	0.	30.
	W_{\odot}	0.	20.
<i>Vertex deviation</i>			
	VD_a	-1	1
	VD_b	-1	1
<i>Thin disc</i>			
	A	4	60
	B	0	60
	C	-0.5	0.5
	σ_V/σ_U	0.3	1.
	σ_W/σ_U	0.3	1.
	h_{σ_U}	1	25.
	h_{σ_W}	1	25.
<i>Thick disc</i>			
	σ_U	25.	80.
	σ_V	25.	80
	σ_W	25.	80
<i>Old thick disc</i>			
	σ_U	25.	80
	σ_V	25.	80
	σ_W	25.	80

5. Results

The values of the fitted parameters are given in table 3, 4 and 5 for the age-velocity dispersion as a fourth order polynomial, square root formula, and power law formula, respectively. The velocity dispersions for the old thick disc are noticeably larger than the one of the young thick disc, as expected from their respective scale heights. It confirms the collapse with time during the thick disc phase, and the probable contraction from

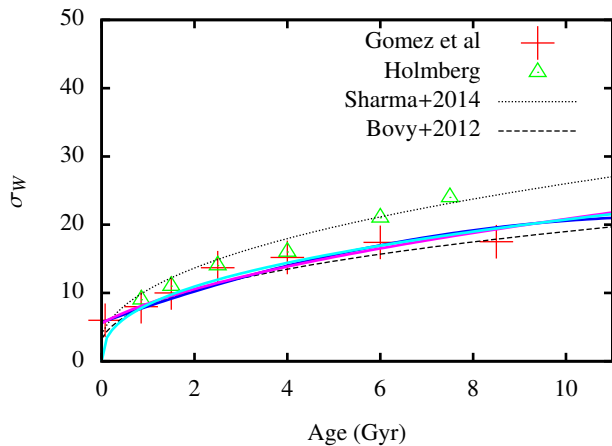


Figure 5. Evolution of the vertical velocity dispersion of the thin disc with age. The solid lines show the best fit solutions for the 3 different formulae (fit 1: blue, 2: magenta, 3: cyan, see text), while the symbols indicate the Gómez et al. (1997) values from Hipparcos (red plus) and Holmberg et al. (2009) (green triangles). Black dotted line is the relation from Sharma et al. (2014) while black dashed line is the one from Bovy et al. (2012).

a larger thick disc with slower rotation in the past towards a smaller and more concentrated thick disc with faster rotation later on.

The Sun velocities are also well constrained by this analysis and we find mean motions in good agreement with previous studies for U and W velocities. For the case of the circular velocity, we got a lower value than found from many other studies. This is discussed in next section.

The thin disc diffusion with time is also constrained to be close to the values obtained by Gómez et al. (1997) from Hipparcos data. Figure 5 shows the comparison between the results of our fits with the 3 assumed formulas, and data from Holmberg et al. (2009) and Gómez et al. (1997). The agreement is good for the young ages with both determinations but is closer to Gómez et al. (1997) for the older stars. We also overplot the velocity dispersion as a function of time obtained by Sharma et al. (2014) and by Bovy et al. (2012) for a further discussion.

To evaluate visually the agreement between model and data we show in Figures 6 histograms for cool stars ($T_{\text{eff}} < 5300\text{K}$) and hot stars ($T_{\text{eff}} > 5300\text{K}$) of radial velocities and proper motions. We clearly see how cool stars present larger velocity dispersions (seen from radial velocity histograms), although in proper motions their dispersions are smaller due to the distance effect in those mostly giant stars.

Histograms of radial velocity and proper motions by metallicity bins are shown in Figure 7 for metallicity range $-1.2 < [M/H] < -0.8$ (dominated by the old thick disc), Figure 8 for $-0.8 < [M/H] < -0.4$ (dominated by the young thick disc), Figure 9 for $-0.4 < [M/H] < 0$ (mainly thin disc), and Figure 10 for $0 < [M/H] < 0.4$ (metal-rich thin disc) respectively. One notices that the fit to each individual population is good, with a higher dispersion for the old thick disc than for the young thick disc, as expected and seen in the dispersion in Table 3. For metal rich stars, the proper motion in declination a slight shift, which could be due to the vertex deviation, expected to be higher in those (in

Table 3. Best values of fitted parameters obtained by the mean of the last third of 8 independent chains and standard deviation assuming Caldwell & Ostriker (1981) and Sofue (2015) rotation curves. Units are km/s for velocities, pc for the scale lengths and radians for the vertex deviation, which is given for stars younger than 1 Gyr (VD_a) and older than 1 Gyr (VD_b). A,B,C are the coefficients of the polynomial describing the variation of σ_W with age in Gyr (Eq. 1). The BIC is computed from Eq. 4.

Parameter	Caldwell	Sofue
<i>Solar motion</i>		
U_{\odot}	12.75 ± 1.26	11.88 ± 1.38
V_{\odot}	0.93 ± 0.30	0.91 ± 0.26
W_{\odot}	7.10 ± 0.16	7.07 ± 0.16
<i>Vertex deviation</i>		
VD_a	-0.0439 ± 0.0375	-0.0618 ± 0.0218
VD_b	-0.0144 ± 0.0122	-0.0048 ± 0.0108
<i>Thin disc</i>		
A	5.69 ± 0.37	5.69 ± 0.41
B	2.48 ± 0.30	2.33 ± 0.28
C	-0.0966 ± 0.0404	-0.0774 ± 0.0362
σ_V/σ_U	0.57 ± 0.03	0.58 ± 0.03
σ_W/σ_U	0.46 ± 0.03	0.46 ± 0.02
h_{σ_U}	$13176. \pm 6908.$	$9534. \pm 3982.$
h_{σ_W}	$15919. \pm 8609.$	$10414. \pm 6299.$
<i>Thick disc</i>		
σ_U	40.02 ± 1.74	41.58 ± 1.51
σ_V	31.86 ± 1.55	30.95 ± 1.50
σ_W	27.89 ± 1.26	27.02 ± 1.00
<i>Old thick disc</i>		
σ_U	75.64 ± 8.58	79.64 ± 7.96
σ_V	55.41 ± 8.74	57.55 ± 8.51
σ_W	66.43 ± 3.95	62.15 ± 6.62
Lr	$-5384. \pm 38.$	$-5378. \pm 155.$
BIC	$10861. \pm 76.$	$10851. \pm 161.$

the mean) younger stars. We shall consider to implement a spiral arm model in the future to investigate and solve this problem.

In order to have a complete view of the agreement of the model in different regions of the sky, histograms of RAVE radial velocities and TGAS proper motions in the 11 sky regions used are presented in the Appendix A, where the data are in solid lines and the model in dashed lines. Figures A.1,A.3 and A.5 show histograms for cool stars, while figures A.2,A.4 and A.6 present similar plots for hot stars. In each figure, the columns indicate the metallicity range used, from $]-1.2;-0.8]$ on the left, to $[0;0.4]$ on the right. Hence the old (metal-weak) thick disc dominates in the first column, the main thick disc in the second column, the main thin disc in the third column, and the metal-rich thin disc dominates in the fourth column.

The histograms show very good agreements between the model and the data in nearly all cases. There is noticeable Poisson noise in the old thick disc (first column) in many cases, which explains why the uncertainties on the parameters of this population are sensitively larger than for the thin (third and fourth columns) and young thick discs (second column). The hotter stars show significantly smaller dispersions than cooler stars in proper motions, which is mainly due to the fact that the giants (cooler) are at larger distances in the mean. One notices also the strong skewness of the distributions in many cases, which explains the necessity to fit the whole histograms and not only the mean and standard deviation of each parameter.

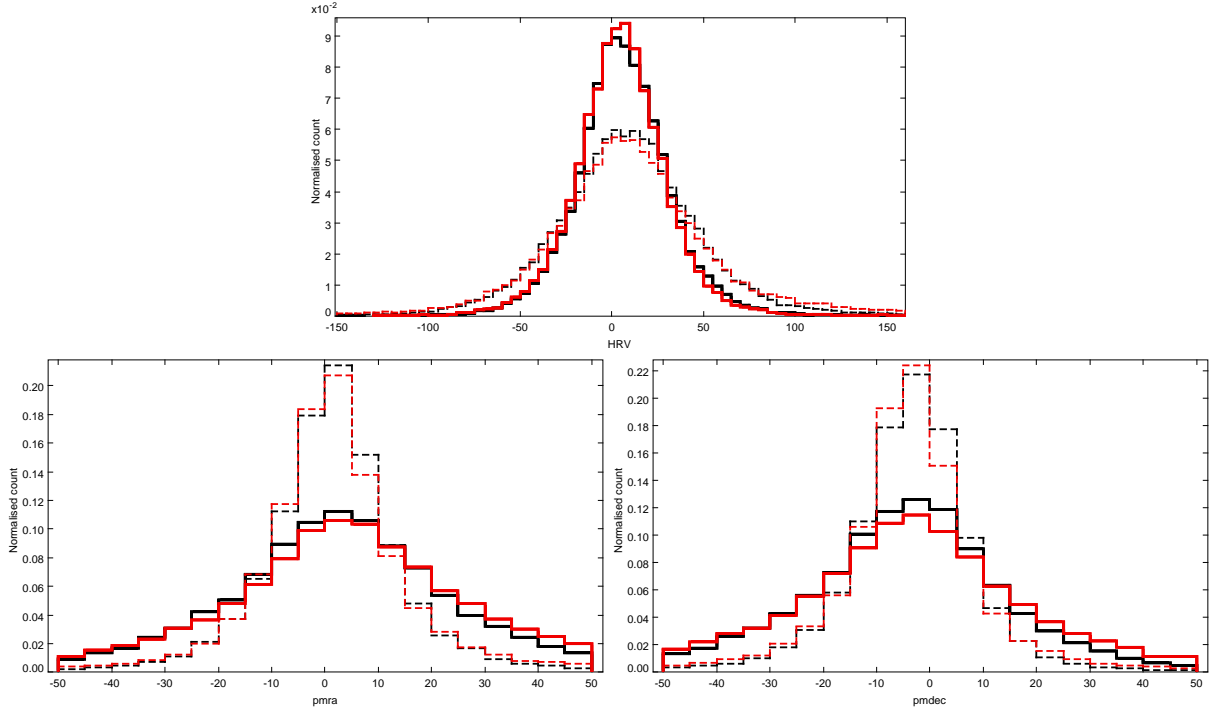


Figure 6. Histograms of RAVE radial velocity distributions (top panel) and TGAS proper motions (bottom panels: left: proper motion along right ascension; right: along declination) for hot (solid lines) and cool (dashed lines) stars. Data: black lines; Best fit model: red lines.

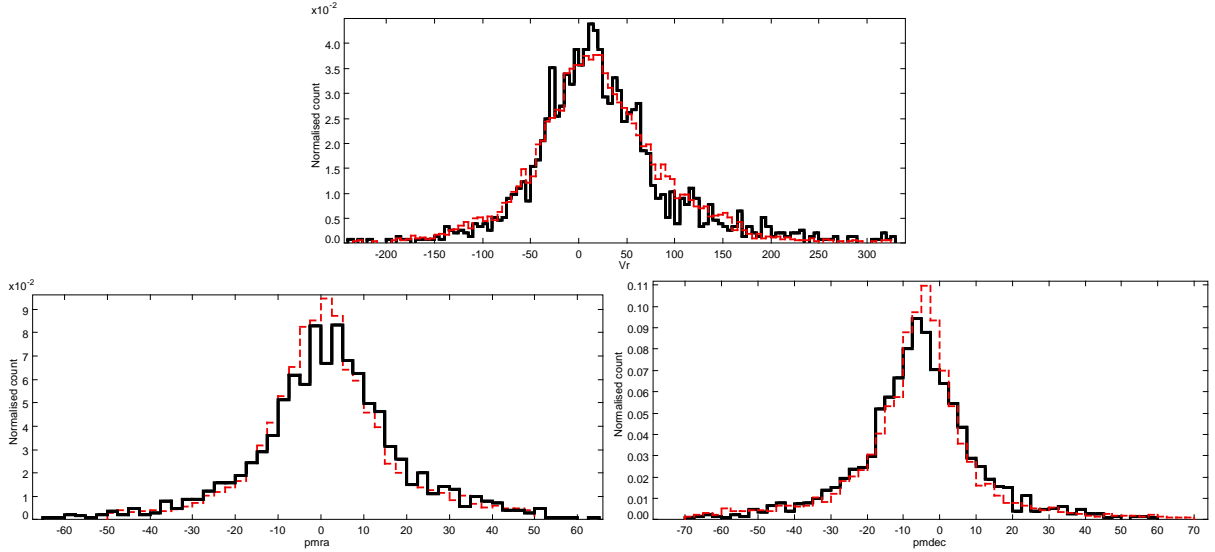


Figure 7. Histograms of RAVE radial velocity distributions (top panel) and TGAS proper motions (bottom panels: left: proper motion along right ascension; right: along declination) for the metallicity bin $-1.2 < b < -0.8$ dex, dominated by the old thick disc. Data: black solid lines; Best fit model: red dashed lines.

Although the global fits are very good, there are a few noticeable difference in some fields which are probably due to some substructures, such as streams, associations or clusters. It is also possible that our vertex deviation does not represent well the real one, and should be better modelled, for example with a spiral arm model. The regions that present systematic deviations with the TGAS proper motions are the South Galactic cap (shift and dispersion in μ_U and μ_V), although the radial velocity dispersion being well reproduced. Even though TGAS

is much more homogeneous and well behaved than previous astrometric surveys, it is not completely free from systematics, as shown by Arenou et al. (2017), especially due to the scanning law and the limited number of observations included in this first release. Future Gaia releases will allow to solve this problem. Towards the Galactic center at intermediate latitudes ($-45 < l < 45$, $25 < b < 40$), there is also a significant disagreement in μ_l , for hot stars. However the fit is nearly perfect in μ_b for all type stars, cool and hot, and any metallicities. Proper

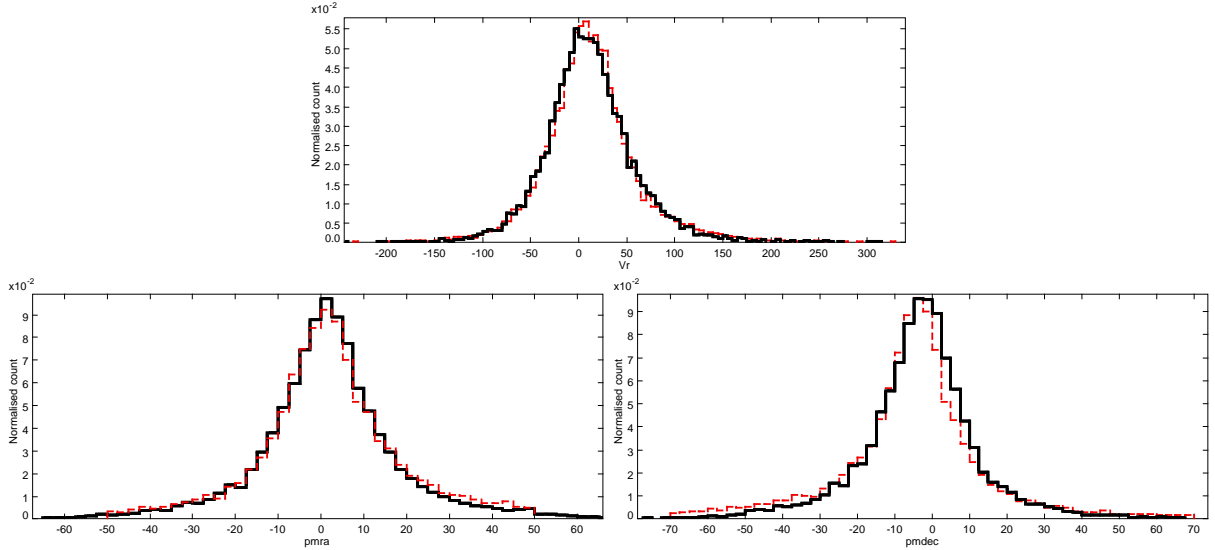


Figure 8. Same as Fig. 7 for the metallicity bin -0.8 to -0.4 dex, dominated by the main thick disc.

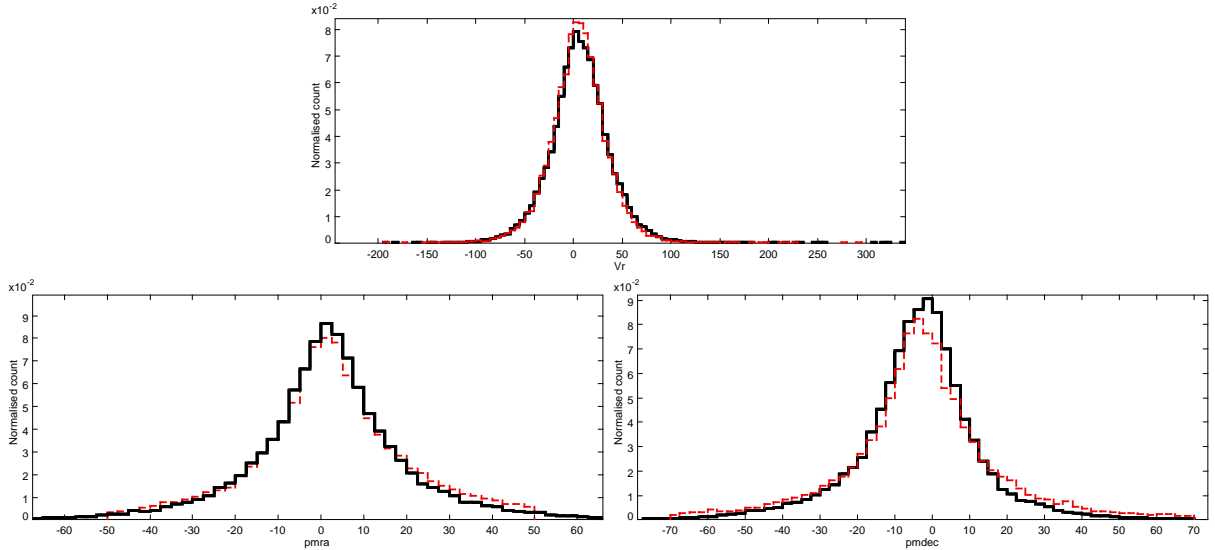


Figure 9. Same as Fig. 7 for the metallicity bin -0.4 to 0 dex, dominated by the main thin disc.

motion histograms of hot stars are also in very good agreement in all directions, however those stars being at larger distances, it might be harder to distinguish significant deviations from an axisymmetric model. Radial velocities from RAVE are very well reproduced by the model, specially for hot stars at all metallicities and in all directions. For low metallicity cool stars, the histograms are noisy because of the small number of stars, but the histograms for high metallicity bins are well reproduced in all regions.

6. Discussion

Compared with previous RAVE analysis, we have used different hypotheses which are improvements and probably give more reliable results. First, we use an improved asymmetric drift which depends explicitly on R_{gal} and z_{gal} and on age, and is consistent with the Galactic potential. Second, we use the metallicity to help distinguish the thin from the thick disc, and

consider separately temperature bins dominated by dwarf and giants resp. Third, we take explicitly into account the selection bias of the data and compare the model simulations in the space of observables. Fourth, we explore the full parameter space and determine also the radial velocity dispersion gradients (or kinematical scale length).

Using this method, we get reliable results for the various tested parameters which describe the kinematics of stellar populations, as discussed below. We discuss separately the V component of the Solar motion which is related to the circular velocity of the LSR, to the rotation curve and to the asymmetric drift.

6.1. U and W component of the Solar motion

We obtain the following values for the Solar motion $U_{\odot} = 13.2 \pm 1.3$ km/s. and $W_{\odot} = 7.1 \pm 0.2$ km/s.

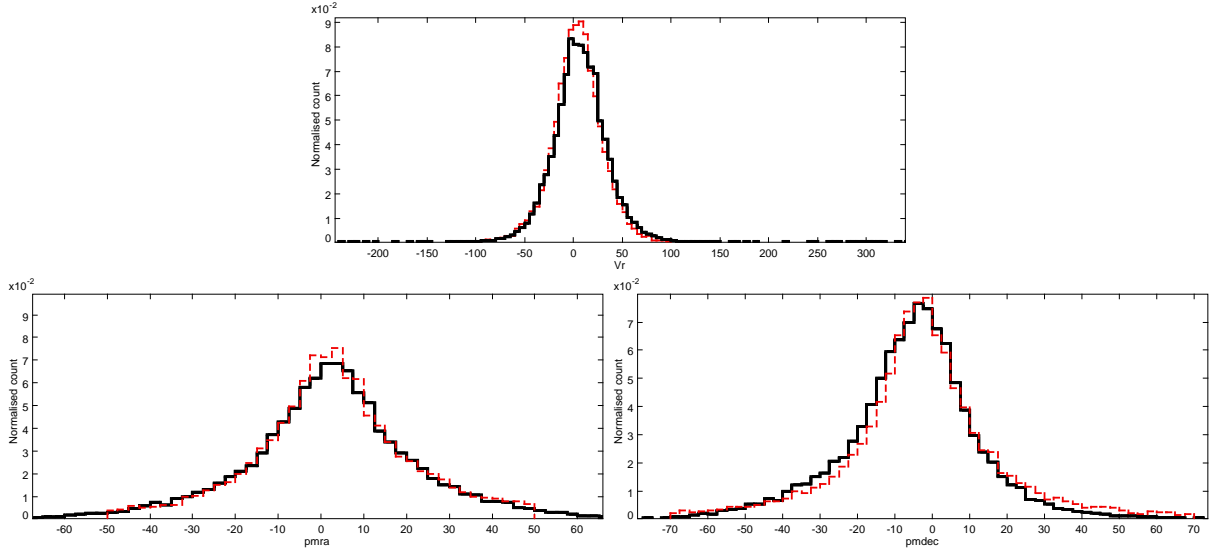


Figure 10. Same as Fig. 7 for the metallicity bin 0 to 0.4 dex, dominated by the metal-rich thin disc.

Table 4. Same as Table 3 but where α and γ are the parameters of the square root function of the velocity dispersion as a function of age in Gyr (Eq. 2).

Parameter	Caldwell	Sofue
<i>Solar motion</i>		
U_{\odot}	12.92 ± 1.14	12.79 ± 0.85
V_{\odot}	0.92 ± 0.21	0.96 ± 0.25
W_{\odot}	7.08 ± 0.14	7.12 ± 0.17
<i>Vertex deviation</i>		
VD_a	-0.0435 ± 0.0148	-0.0458 ± 0.0152
VD_b	-0.0148 ± 0.0087	-0.0133 ± 0.0064
<i>Thin disc</i>		
α	32.33 ± 1.96	32.23 ± 1.89
γ	40.41 ± 2.74	42.55 ± 2.38
σ_V/σ_U	0.57 ± 0.03	0.57 ± 0.03
σ_W/σ_U	0.46 ± 0.02	0.47 ± 0.02
h_{σ_U}	$7493. \pm 7009.$	$14776. \pm 7946.$
h_{σ_W}	$8578. \pm 5896.$	$16432. \pm 9622.$
<i>Thick disc</i>		
σ_U	39.05 ± 3.04	41.23 ± 1.56
σ_V	32.31 ± 1.44	32.90 ± 1.87
σ_W	28.61 ± 1.27	26.92 ± 1.12
<i>Old thick disc</i>		
σ_U	80.03 ± 10.92	81.31 ± 8.73
σ_V	57.35 ± 7.29	57.98 ± 7.46
σ_W	61.89 ± 6.09	59.03 ± 8.25
Lr	$-5395. \pm 42.$	$-5417. \pm 29.$
BIC	$10874 \pm 85.$	$10916. \pm 58.$

Table 5. Same as Table 3 but where k and β are the parameters of the power law function of the velocity dispersion as a function of age in Gyr (Eq. 3).

Parameter	Caldwell	Sofue
<i>Solar motion</i>		
U_{\odot}	13.00 ± 1.02	13.12 ± 1.47
V_{\odot}	0.94 ± 0.23	0.92 ± 0.29
W_{\odot}	7.01 ± 0.15	7.03 ± 0.18
<i>Vertex deviation</i>		
VD_a	-0.0325 ± 0.0131	-0.0388 ± 0.0126
VD_b	-0.0173 ± 0.0075	-0.0167 ± 0.0111
<i>Thin disc</i>		
k	8.30 ± 0.19	8.26 ± 0.22
β	0.40 ± 0.02	0.40 ± 0.02
σ_V/σ_U	0.54 ± 0.02	0.57 ± 0.03
σ_W/σ_U	0.46 ± 0.02	0.47 ± 0.02
h_{σ_U}	$19430. \pm 3948.$	$13009. \pm 8856.$
h_{σ_W}	$11813. \pm 8010.$	$10473. \pm 7058.$
<i>Thick disc</i>		
σ_U	40.36 ± 2.00	42.18 ± 2.05
σ_V	32.85 ± 1.44	32.26 ± 2.06
σ_W	27.03 ± 1.20	26.90 ± 1.10
<i>Old thick disc</i>		
σ_U	80.30 ± 10.32	75.87 ± 5.52
σ_V	57.81 ± 6.35	53.93 ± 5.87
σ_W	62.24 ± 5.25	66.22 ± 3.23
Lr	-5429 ± 32	$-5420. \pm 31.$
BIC	10942 ± 65	$10923. \pm 62.$

For the U_{\odot} velocity, our value is well in agreement with previous results (Aumer & Binney (2009): 9.96 ± 0.33 , Schönrich et al. (2010): 11.1 ± 0.7 , Coşkunoğlu et al. (2011): 8.5 ± 0.4 km/s, Pasetto et al. (2012a): 9.87 ± 0.37 km/s, Karaali et al. (2014): 10 km/s, Sharma et al. (2014): 11.45 ± 0.1 , Bobylev & Bajkova (2015): 6.0, Bobylev & Bajkova (2016): 9.12). The error bars do not generally take into account the systematics due to the model used. But the latter reference noted a slight degeneracy between U and V solar motion, due to the portion of sky covered by RAVE.

The vertical solar motion is more reliably determined in most of the studies, with consistent values of the order of 7 ± 1 km/s. We confirm this value.

6.2. Thin disc velocity ellipsoid and gradients

Also studying the RAVE survey, Williams et al. (2013) restricted their analysis to red clump stars. They studied in particular the differences between north and south, looking for non-axisymmetry, which we do not do. Evidences of non-

axisymmetries were already pointed out by Siebert et al. (2011a) in the analysis of RAVE third data release (Siebert et al. 2011b). We shall dedicate such an analysis to a future paper. In their figure Williams et al. (2013) found that the asymmetric drift varies with z_{gal} by about 40 km/s between $z_{\text{gal}}=0$ and $z_{\text{gal}}=2$ kpc, which is in good agreement with our model. Also in agreement, the lag in V_ϕ at the $z_{\text{gal}}=0$ is approximately constant with R_{gal} . These studies did not investigate the dependency of the velocity ellipsoid with age, as we do.

In their study of a RAVE internal data release, intermediate between DR3 and DR4, Pasetto et al. (2012b) performed a detailed analysis of the velocity ellipsoid and cross-terms of the velocity dispersion and their variation with R_{gal} and z_{gal} . Similarly to our study, they did not find any evidence of variations with R_{gal} most probably because the RAVE sample is not deep enough to reach regions where the sensitivity to R_{gal} can be significant. In this study, the mean velocity dispersions for the thin disc component were found to be (26, 20, 16) along U, V, W components resp. which is in good agreement with our values, according to the fact that we study its variation with age, while they do not. Their values are close to the values for the old thin disc.

Sharma et al. (2014) investigated the disc kinematics from GCS and RAVE data analysis with a MCMC method, but with considerable differences with us in the assumptions and in the fitting method. They used parameters from an older stellar population model (Robin et al. 2003) introduced in the Galaxia model Sharma et al. (2011). Similar density laws are assumed for the thin and thick discs, but we have shown in Robin et al. (2014) that the parameters of the thick disc in Robin et al. (2003) are not accurate, although the impact of this assumption on their analysis might be minor. They tested distributions in velocities to be Gaussian or Shu's distributions, and used the asymmetric formula proposed by Bovy et al. (2012). On the other hand they assumed that the asymmetric drift does not depend on distance to the plane, contrarily to our study. They also fixed the scale length of the disc to be 2.5 kpc for both the thin and thick disc. While we used a scale length of 2.53 kpc for the thin disc, our thick disc was split into an old component of scale length 3 kpc and a younger component of scale 2 kpc. Contrarily to them, we decided not to use GCS survey for constraining the populations. For GCS survey it is more difficult to simulate correctly the selection function, which can introduce critical biases. Sharma et al. (2014) study resulted in similar Sun velocities in U and W , but slightly higher thin disc maximum vertical velocity dispersion of 25 km/s. Figure 5 shows how it compares with Holmberg et al. (2009), Gómez et al. (1997) data and with Bovy et al. (2012)'s model. Sharma et al. (2014) maximum velocity for the thin disc is noticeably larger than our result, and the ones of Bovy et al. (2012) and Gómez et al. (1997).

6.3. Thick disc velocity ellipsoid

Our study points towards a σ_z of 28 km/s for the young thick disc, and 59 km/s for the old thick disc. It is in fair agreement with most previous studies, although they generally do not separate the thick disc in this way.

Guiglion et al. (2015) analyzed the Gaia-ESO Survey in order to study the dependency of the velocity dispersions with metallicities and abundances. The correspondance of the α abundance ratio with age should in principal lead to estimate the age-velocity dispersion relation. However this correspondance is only qualitative for the time being. They show that the velocity dispersion increases with α , with at high α a higher value for

lower metallicities ($[\text{Fe}/\text{H}] \approx -0.80$) than at typical thick disc metallicity ($[\text{Fe}/\text{H}] \approx -0.53$). We find similar results, although our lowest metallicity bin has a velocity dispersion σ_W of 59 km/s, while they have only about 50 km/s. For the standard thick disc with mean $[\text{Fe}/\text{H}]$ of -0.5 we have σ_W of 27 km/s, while they have about 35 km/s from their figure 9. However it is difficult to compare with the present result which explores extensively the model parameter space, and because the selection function is very different between Gaia ESO survey and RAVE-TGAS data set. But in general terms, both studies find similar trend of σ_W with $[\text{Fe}/\text{H}]$ for the high α population.

In a RAVE internal data release, Pasetto et al. (2012a) found a mean thick disc asymmetric drift of 49 km/s, in agreement with our model, where the lag depends explicitly on z_{gal} . In figure 4 we see that in our model the thick disc lag reaches this value at z_{gal} about 1.5-2 kpc at the solar radius. In their study the velocity ellipsoid of the thick disc is (56, 46, 35) which is in between the two thick disc components in the present study.

6.4. Solar circular velocity, asymmetric drift and rotation curve

V_\odot in particular has been widely discussed in the literature. Values range between about 5 km/s and 26 km/s. Among the most recent studies, Binney (2010) study based on GCS and SDSS data points towards 11 km/s, Schönrich et al. (2010) also from GCS towards 12.24 ± 0.5 km/s but with a sensitively different model. On the lower side limit, Aumer & Binney (2009) used Hipparcos data and found $V_\odot = 5.25 \pm 0.54$ km/s, while Bovy et al. (2012), using preliminary APOGEE data (first year release) obtained 26 ± 3 km/s, however with a large value of $V_{\text{LSR}} + V_\odot = 242$ km/s.

Using a RAVE internal data release with 402 721 stars, close to the final DR4, Golubov et al. (2013) found $V_\odot = 3$ km/s using a new formulation of the Strömberg relation. From the final RAVE-DR4, Karaali et al. (2014) analysed the dependency of the determination of V_\odot on Z coordinate and found a minimum of ≈ 10 km/s in the plane. Wojno et al. (2016) studied the chemical separation of disc components. They showed the dependency of the asymmetric drift (their fig 4ab) with $[\text{Fe}/\text{H}]$, drastically different for thin and thick components defined according to their $[\text{Mg}/\text{Fe}]$ abundances. They assume the solar motion from Schönrich et al. (2010). Their result is difficult to compare with the present work. In our case the asymmetric drift is not a fitted parameter, and contrarily to Wojno et al. (2016), it depends strongly on distance from the plane. Our values might also depend on metallicity via the age-vertical velocity dispersion relation but this one is not well known for the thick disc. Jing et al. (2016) with LAMOST data, separating disc components based on the eccentricity of orbits obtained similar results to Wojno et al. (2016).

Bobylev & Bajkova (2015) determined the Solar motion from a local sample of young objects including masers and found $V_\odot = 6.5$ km/s. On the other hand, the same authors Bobylev & Bajkova (2016) obtained quite significantly different values from the analysis of RAVE-DR4, based on Bottlinger's formulas and determination of the distribution of stars in the (U, V) plane using wavelet transform. U_\odot and V_\odot velocities were computed using UCAC4 proper motions and distances estimated by Binney et al. (2014). They find $V_\odot = 20.8$ but with V_\odot changing a lot with age and distance to the plane.

Sharma et al. (2014) obtained a range of values depending whether they use Gaussian or Shu distributions, and on the degeneracies between parameters. An important point is the

fact that they do not distinguish easily the different populations, while we are using metallicity and temperature to separate them.

It should be noted that all investigations of the Sun circular velocity are not done independently from assumptions or evaluations of the rotation curve and from the assumed asymmetric drift. Even the rotation curve at the Sun position is subject to debate. In studies based on local data what matters is whether the rotation curve is flat, decreasing or increasing at the Sun position.

A preliminary analysis of the rotation curve from Gaia-TGAS data has been conducted by Bovy (2017) from a completely different approach from the one that we undertake in our study. Their analysis did not solve for the Solar motion and assumed the solar velocities from Schönrich et al. (2010). They presented the Oort's constant measurements and emphasized that the rotation curve is slightly decreasing at the Sun Galactocentric radius. This is compatible with the rotation curves used in the present study.

Moreover, its determination using different tracers varies, due to neglected deviations from circular motion, or from neglected or unknown asymmetric drift variations with R_{gal} and z_{gal} . While it is well known and described for stars in the Galactic plane (Oort 1965), its variation with z_{gal} depends on the shape of the potential as well as on the cross terms of the velocity ellipsoids. At the notable exception of Binney (2010), in other works the dependency of the asymmetric drift with z is not done, neither empirically nor in a dynamically consistent way. This directly impacts these studies when they estimate of the velocity of the Sun relatively to the LSR. In the present work, taking into account the strong variation of the asymmetric drift with z_{gal} dynamically self-consistently, we find that the Solar circular velocity has been overestimated in previous studies.

6.5. Radial gradients of velocity dispersion

We attempted to constrain the radial gradient of σ_U and σ_W inside the thin disc population, as they are ingredients of the asymmetric formula in the Galactic plane and can be related to the density scale length. However, we did not succeed to get this constrain, the standard deviation of our determination being much too large, probably because the range of Galactocentric distances available in RAVE and TGAS are too restricted to the Solar vicinity. We shall consider this point further when the Gaia DR2 will be available.

6.6. Vertex deviation

Our fit included a vertex deviation, assuming two different values, for stars younger and older than 1 Gyr. Our result points towards a slight vertex deviation, but only at the 2 sigma level, slightly higher for young stars than for older stars. This is not a strong signal that we do not discuss further.

7. Conclusions

In the approach that we present here, we use a full description of the asymmetric drift for each sub-component of the BGM as a function of R_{gal} and z_{gal} , consistently with the velocity ellipsoid. This analysis shows that this lag is very important and varies strongly with z_{gal} and slightly with R_{gal} . The comparison of the fitted histograms of radial velocity and proper motions shows that this method is efficient to reproduce the kinematics in a wide solar neighbourhood. We draw the following conclusions:

- The self consistent description of the velocity ellipsoid based on an approximation of the Stäckel potential provides a very efficient way to model the stellar kinematics in a wide region around the Sun. It reproduces very well the behaviors seen in RAVE and TGAS surveys.
- We provide new determinations of the Solar motion, which confirms already known values of the velocity components U and W and propose a new value of the Solar velocity towards rotation.
- We confirm the secular evolution of the velocity dispersion at the Sun found from Hipparcos data by Gómez et al. (1997).
- We do not obtain a strong constrain on the kinematics scale length. This requires further investigations using data at larger distances from the Sun. We are considering using APOGEE, GaiaESO and future Gaia releases for this purpose.
- From these data alone, the constraint on the vertex deviation is not severe. A further investigation using next Gaia releases is required.

Hence, the combination of spectroscopic surveys providing accurate radial velocities (RAVE) with Gaia proper motions provide a strong revision of our view of the kinematics at the Solar neighbourhood. We expect from future Gaia data releases to be able to extend this study further away, to measure the kinematical gradients in particular and provide new constraints on the whole Galactic potential and to its approximation by Stäckel potentials.

Acknowledgements. We are grateful to Francesca Figueras, Arnaud Siebert and Benoit Famaey for fruitful discussions. We acknowledge the financial support from "Programme National Cosmologie et Galaxies" (PNCG) of CNRS/INSU, France. BGM simulations were executed on computers from the Utinam Institute of the Université de Franche-Comté, supported by the Région de Franche-Comté and Institut des Sciences de l'Univers (INSU).

JGFT acknowledges support by the CNES (Centre National d'Etudes Spatiales) and by the Région de Franche-Comté.

Funding for RAVE has been provided by: the Australian Astronomical Observatory; the Leibniz-Institut fuer Astrophysik Potsdam (AIP); the Australian National University; the Australian Research Council; the French National Research Agency; the German Research Foundation (SPP 1177 and SFB 881); the European Research Council (ERC-StG 240271 Galactica); the Instituto Nazionale di Astrofisica at Padova; The Johns Hopkins University; the National Science Foundation of the USA (AST-0908326); the W. M. Keck foundation; the Macquarie University; the Netherlands Research School for Astronomy; the Natural Sciences and Engineering Research Council of Canada; the Slovenian Research Agency; the Swiss National Science Foundation; the Science & Technology Facilities Council of the UK; Opticon; Strasbourg Observatory; and the Universities of Groningen, Heidelberg and Sydney. The RAVE web site is at <https://www.rave-survey.org>.

This work has made use of data from the European Space Agency (ESA) mission Gaia (<http://www.cosmos.esa.int/gaia>), processed by the Gaia Data Processing and Analysis Consortium (DPAC, <http://www.cosmos.esa.int/web/gaia/dpac/consortium>). Funding for the DPAC has been provided by national institutions, in particular the institutions participating in the Gaia Multi-lateral Agreement.

Appendix A: Comparison of best model histograms with data

We present histograms of radial velocities and proper motions in the 11 sky regions, comparing our best fit model with real data. We separate stars by temperature, cool stars having $T_{\text{eff}} < 5200\text{K}$ and hot stars $T_{\text{eff}} \geq 5200\text{K}$. In each figure, the columns correspond to different metallicity bins of width 0.4 dex from metal-weak thick disc [-1.2; -0.8] in the first column, [-0.8; -0.4] dominated by the main thick disc in the second column, [-0.4; 0] in majority the main thin disc in the third column, and [0; 0.4] the metal-rich thin disc in the fourth column. At the Galactic

cap, the first and second components of the proper motions are parallel to U and V velocities resp. In other fields, the first and second components of the proper motions are the usual μ_l^* and μ_b in mas/yr. We only present the results obtained with the first age-velocity dispersion (Eq. 1), as the other formulae give very similar results.

References

- Adibekyan, V. Z., Figueira, P., Santos, N. C., et al. 2013, *A&A*, 554, A44
Ahn, C. P., Alexandroff, R., Allende Prieto, C., et al. 2014, *ApJS*, 211, 17
Arenou, F., Luri, X., Babusiaux, C., et al. 2017, *A&A*, 599, A50
Aumer, M., Binney, J., & Schönrich, R. 2016, *MNRAS*, 462, 1697
Aumer, M. & Binney, J. J. 2009, *MNRAS*, 397, 1286
Bienaymé, O., Robin, A. C., & Crézé, M. 1987, *A&A*, 180, 94
Bienaymé, O., Robin, A. C., & Famaey, B. 2015, *A&A*, 581, A123
Binney, J. 2010, *MNRAS*, 401, 2318
Binney, J., Burnett, B., Kordopatis, G., et al. 2014, *MNRAS*, 437, 351
Binney, J. & Tremaine, S. 2008, *Galactic Dynamics: Second Edition* (Princeton University Press)
Bobylev, V. V. & Bajkova, A. T. 2015, *Baltic Astronomy*, 24, 51
Bobylev, V. V. & Bajkova, A. T. 2016, *Astronomy Letters*, 42, 90
Bovy, J. 2017, *MNRAS*, 468, L63
Bovy, J., Allende Prieto, C., Beers, T. C., et al. 2012, *ApJ*, 759, 131
Caldwell, J. A. R. & Ostriker, J. P. 1981, *ApJ*, 251, 61
Coşkunoğlu, B., Ak, S., Bilir, S., et al. 2011, *MNRAS*, 412, 1237
Crézé, M. & Robin, A. 1983, in *IAU Colloq. 76: Nearby Stars and the Stellar Luminosity Function*, ed. A. G. D. Philip & A. R. Uppgren, Vol. 76, 391
Czekaj, M. A., Robin, A. C., Figueras, F., Luri, X., & Haywood, M. 2014, *A&A*, 564, A102
Dehnen, W. & Binney, J. J. 1998, *MNRAS*, 298, 387
Eisenstein, D. J., Weinberg, D. H., Agol, E., et al. 2011, *AJ*, 142, 72
Gaia Collaboration, Brown, A. G. A., Vallenari, A., et al. 2016, *A&A*, 595, A2
Golubov, O., Just, A., Bienaymé, O., et al. 2013, *A&A*, 557, A92
Gómez, A. E., Grenier, S., Udry, S., et al. 1997, in *ESA Special Publication, Vol. 402, Hipparcos - Venice '97*, ed. R. M. e. a. Bonnet, 621–624
Guiglion, G., Recio-Blanco, A., de Laverny, P., et al. 2015, *A&A*, 583, A91
Hayden, M. R., Holtzman, J. A., Bovy, J., et al. 2014, *AJ*, 147, 116
Haywood, M., Di Matteo, P., Lehnert, M. D., Katz, D., & Gómez, A. 2013, *A&A*, 560, A109
Holmberg, J., Nordström, B., & Andersen, J. 2009, *A&A*, 501, 941
Jing, Y., Du, C., Gu, J., et al. 2016, *MNRAS*, 463, 3390
Karaali, S., Bilir, S., Ak, S., et al. 2014, *PASA*, 31, e013
Kordopatis, G., Gilmore, G., Steinmetz, M., et al. 2013, *AJ*, 146, 134
Kunder, A., Kordopatis, G., Steinmetz, M., et al. 2017, *AJ*, 153, 75
Marin, J., Pudlo, P., Robert, C., & Ryder, R. 2011, *Statistics and Computing*, 1
Nordström, B., Mayor, M., Andersen, J., et al. 2004, *A&A*, 418, 989
Norris, J., Bessell, M. S., & Pickles, A. J. 1985, *ApJS*, 58, 463
Oort, J. H. 1965, in *Galactic Structure*, ed. A. Blaauw & M. Schmidt, 455
Pasetto, S., Grebel, E. K., Zwitter, T., et al. 2012a, *A&A*, 547, A70
Pasetto, S., Grebel, E. K., Zwitter, T., et al. 2012b, *A&A*, 547, A71
Randich, S., Gilmore, G., & Gaia-ESO Consortium. 2013, *The Messenger*, 154, 47
Robin, A. C., Reylé, C., Derrière, S., & Picaud, S. 2003, *A&A*, 409, 523
Robin, A. C., Reylé, C., Fliri, J., et al. 2014, *A&A*, 569, A13
Schönrich, R., Binney, J., & Dehnen, W. 2010, *MNRAS*, 403, 1829
Schwarz, G. 1978, *Annals of statistics*, 6, 461,464
Sharma, S., Bland-Hawthorn, J., Binney, J., et al. 2014, *ApJ*, 793, 51
Sharma, S., Bland-Hawthorn, J., Johnston, K. V., & Binney, J. 2011, *ApJ*, 730, 3
Siebert, A., Famaey, B., Minchev, I., et al. 2011a, *MNRAS*, 412, 2026
Siebert, A., Williams, M. E. K., Siviero, A., et al. 2011b, *AJ*, 141, 187
Sofue, Y. 2015, *PASJ*, 67, 75
Wielen, R. 1977, *A&A*, 60, 263
Williams, M. E. K., Steinmetz, M., Binney, J., et al. 2013, *MNRAS*, 436, 101
Wojno, J., Kordopatis, G., Steinmetz, M., et al. 2016, *MNRAS*, 461, 4246

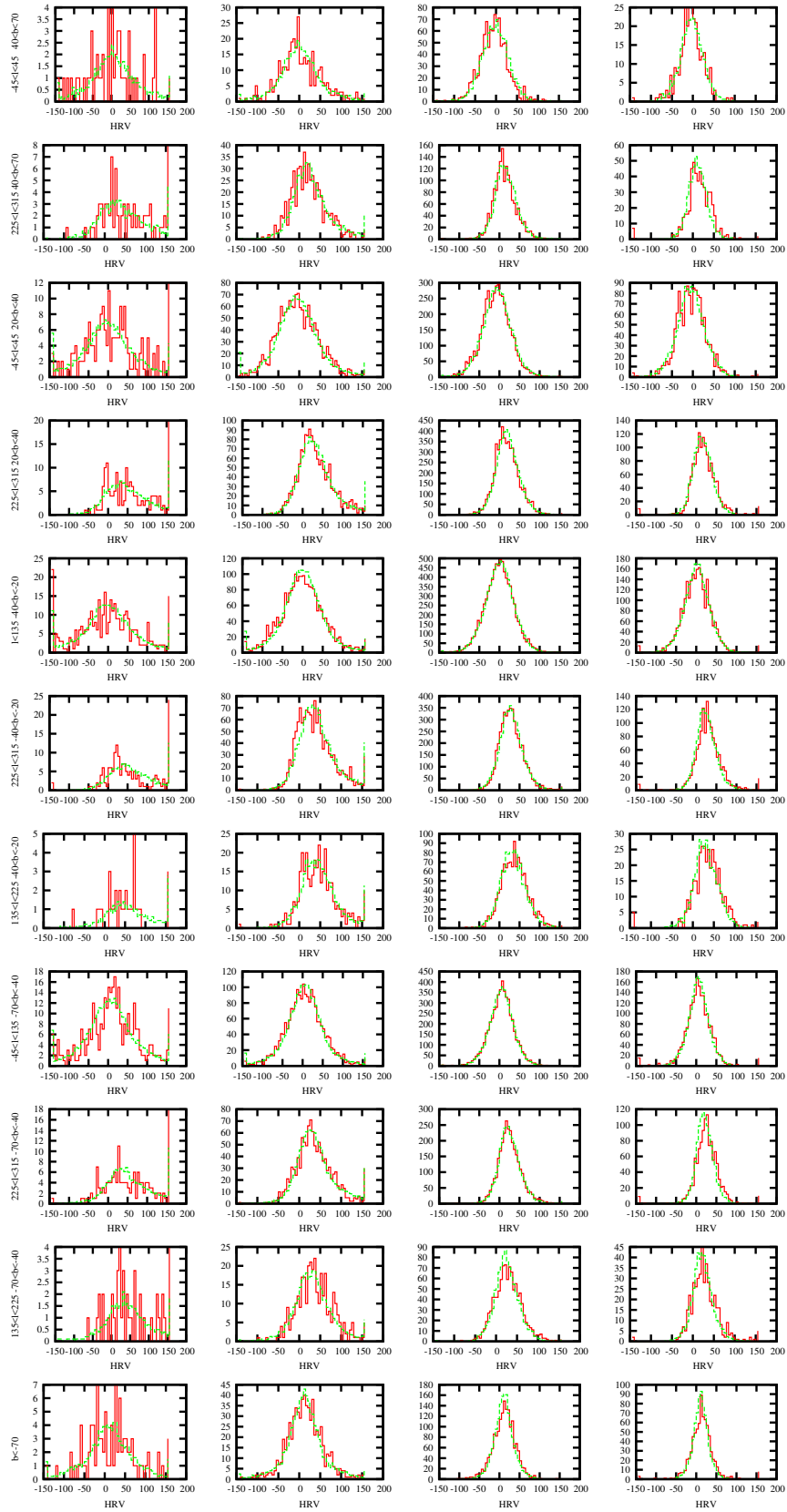


Figure A.1. Histograms of RAVE radial velocity distributions in different sky regions and for different metallicity bins, from -1.2 to 0.4 by steps of 0.4 dex, for cool stars, with 5 km/s bin size. Data: red solid lines; Best fit model: green dashed lines.

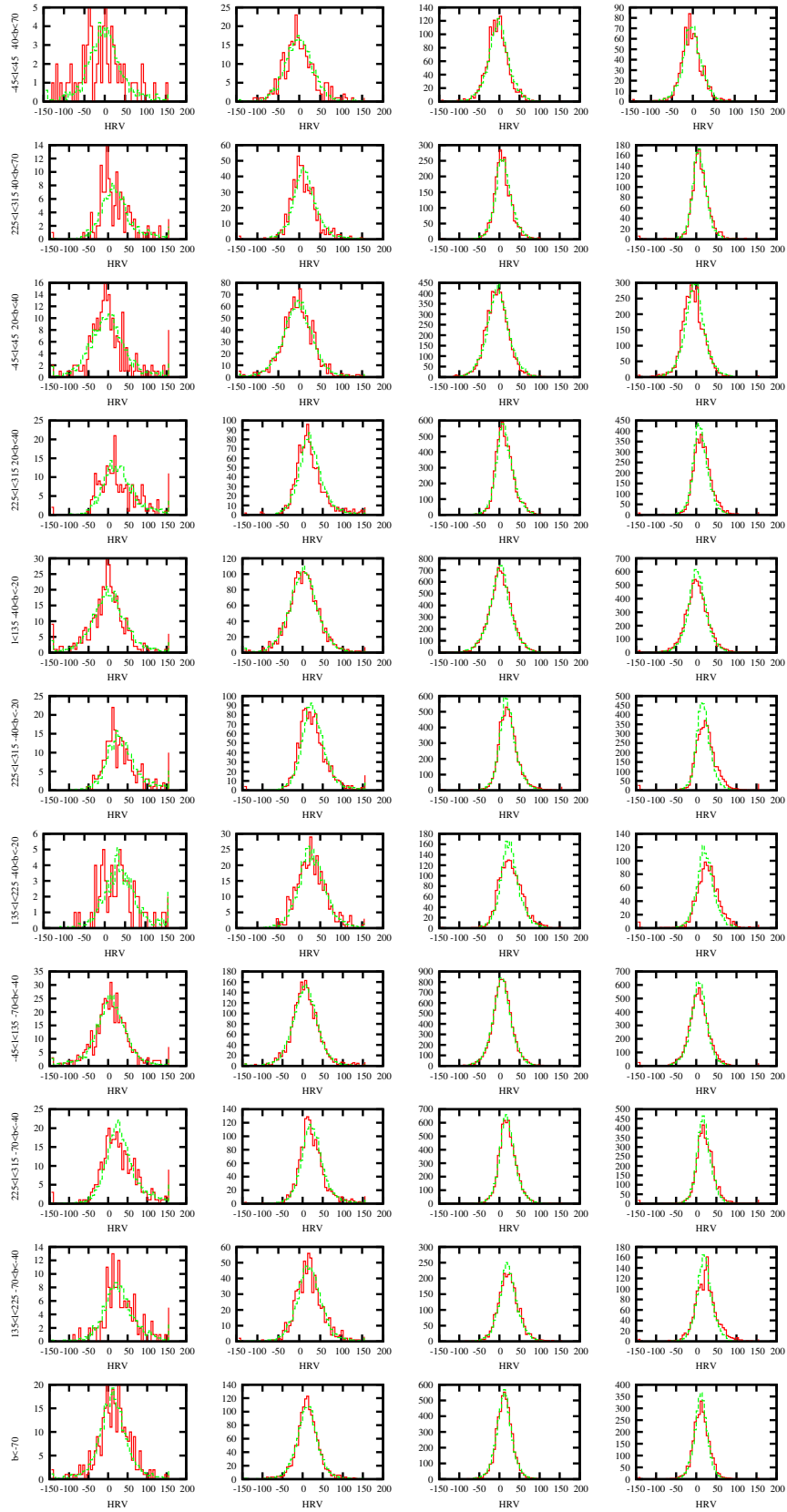


Figure A.2. Same as fig. A.1 but for hot stars.

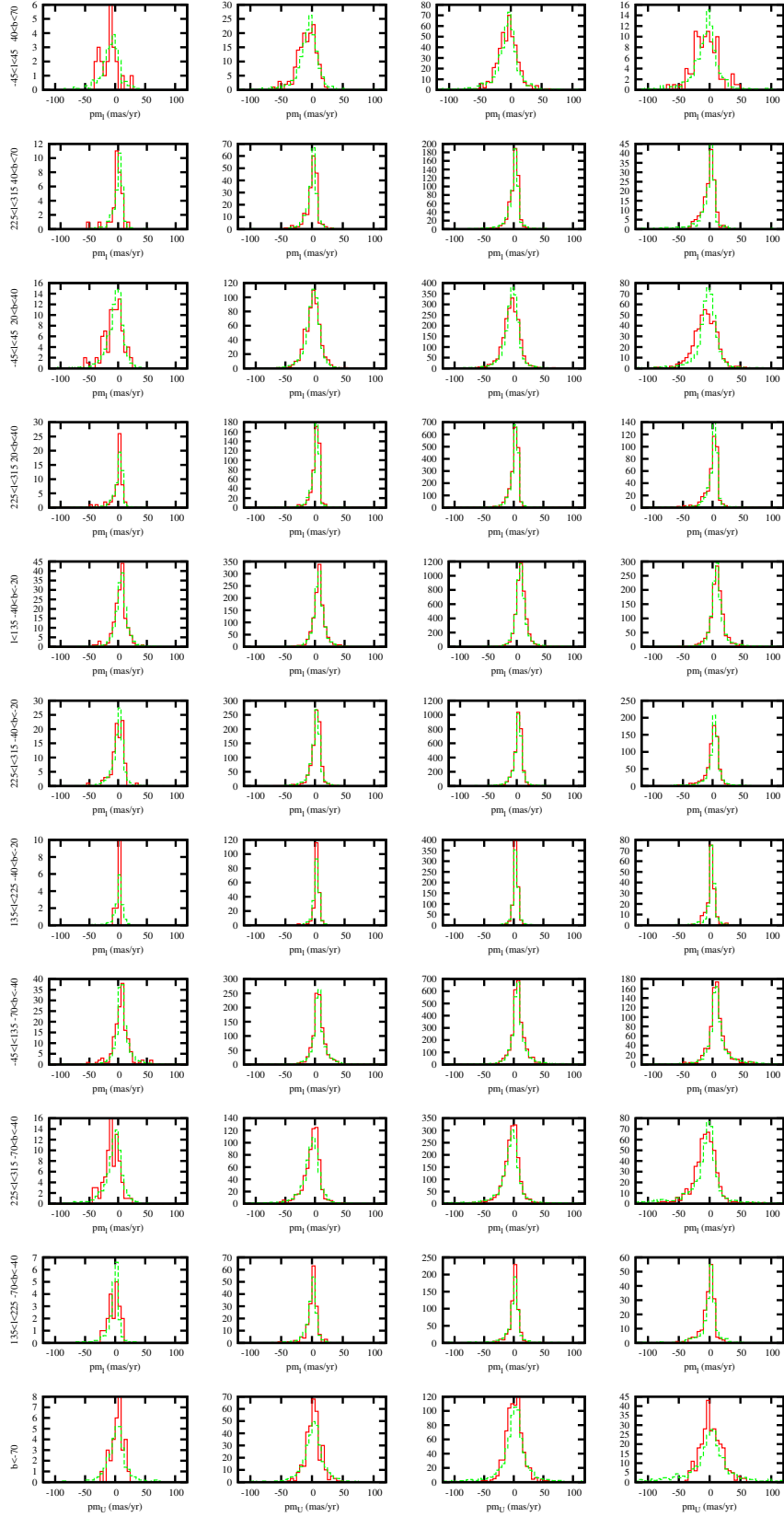


Figure A.3. Histograms of first component of the TGAS proper motion distributions in different sky regions and for different metallicity bins (see fig. A.1), for cool stars, in 5 mas/yr bin size. Data: red solid lines; Best fit model: green dashed lines.

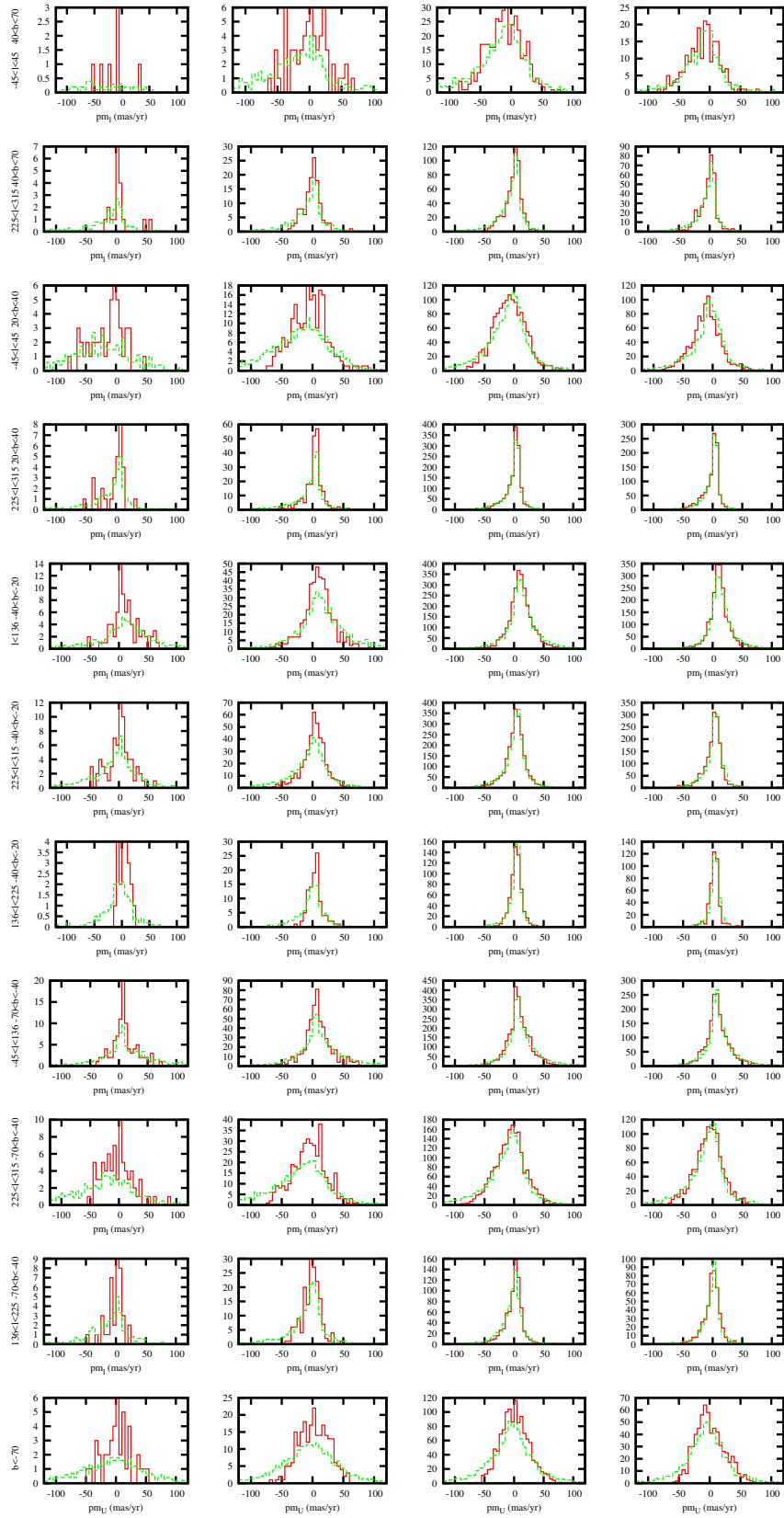


Figure A.4. Same as fig. A.3 but for hot stars.

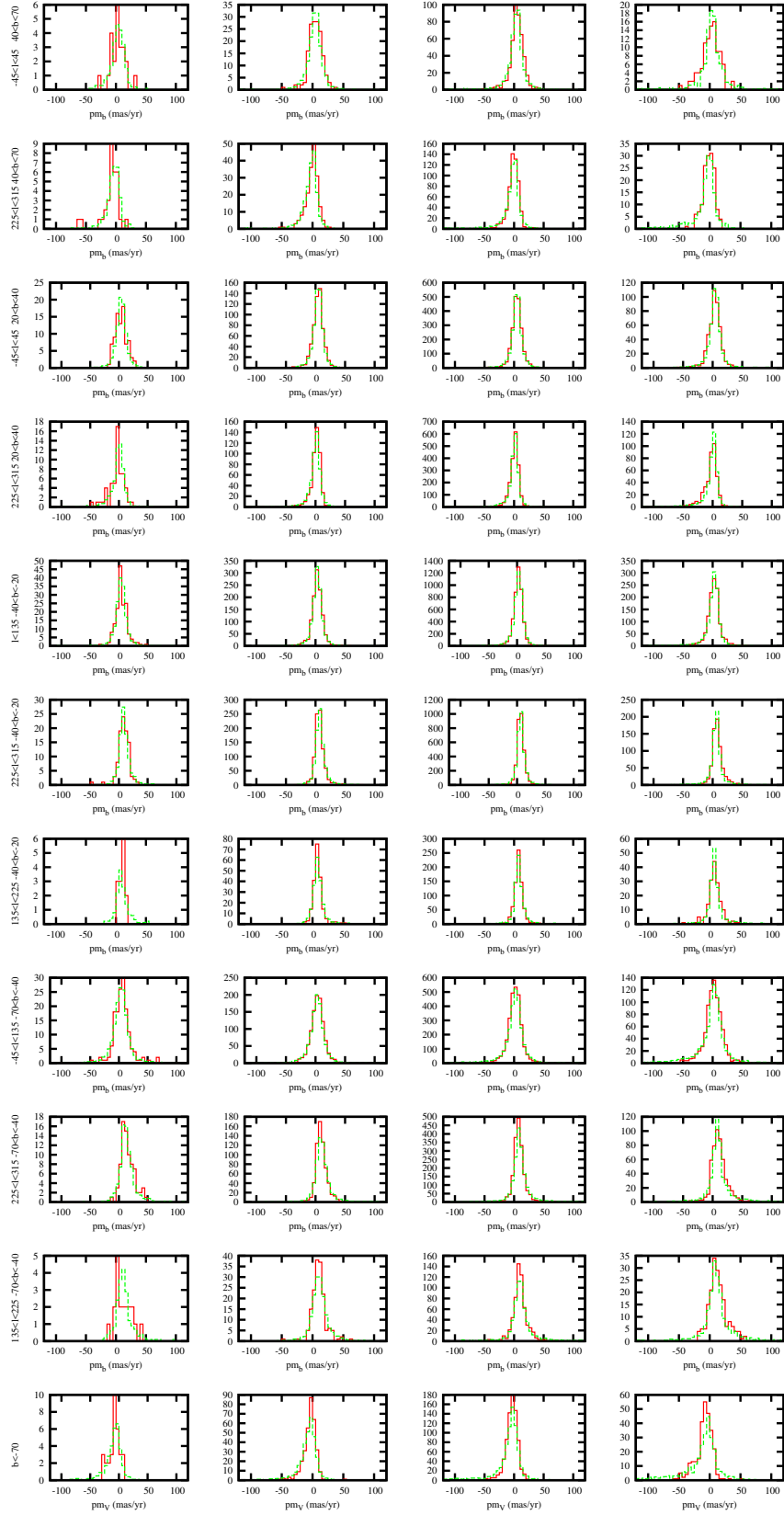


Figure A.5. Histograms of second component of the TGAS proper motion distributions in different sky regions and for different metallicity bins (see fig. A.1), for cool stars, in 5 mas/yr bin size. Data: red solid lines; Best fit model: green dashed lines.

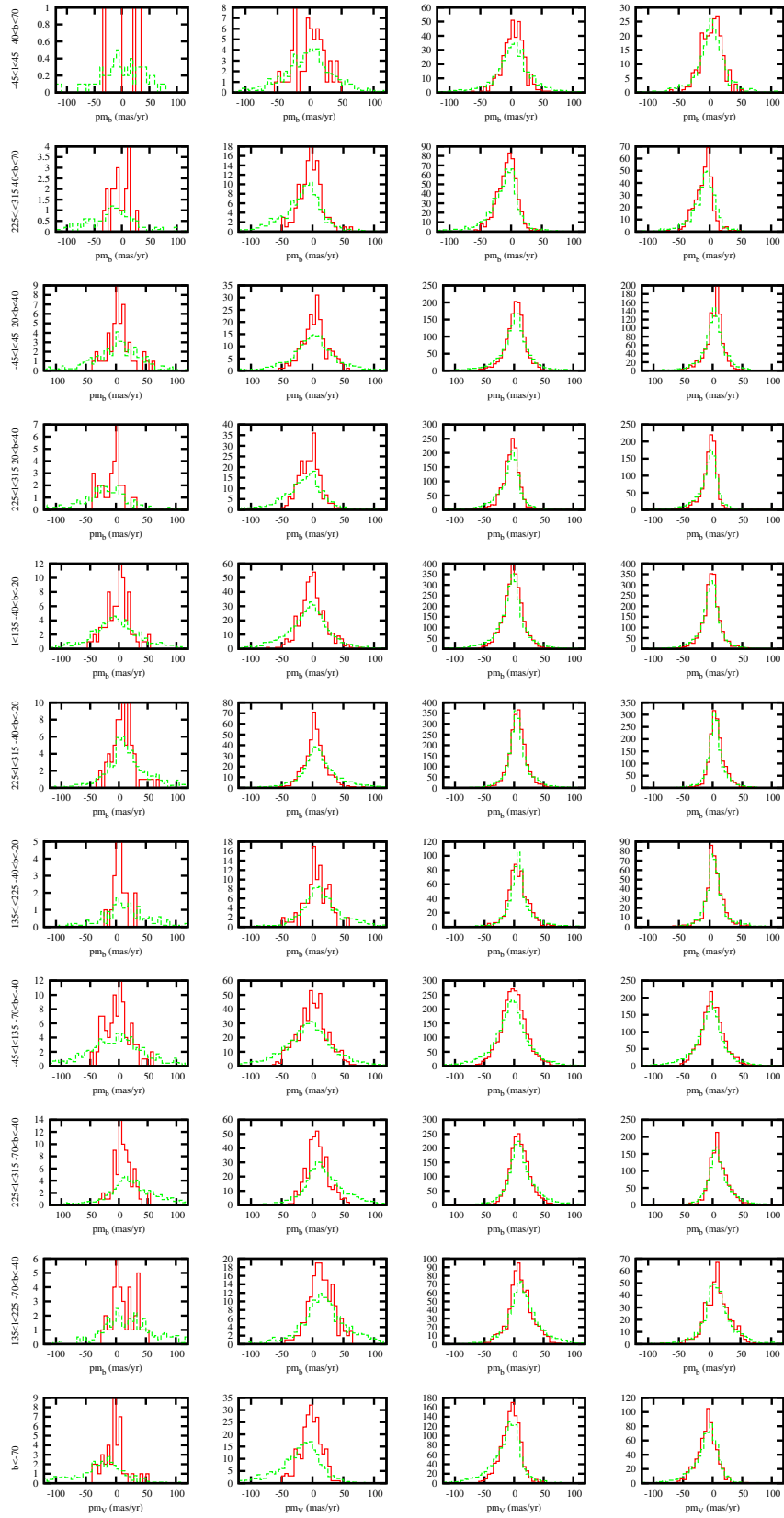


Figure A.6. Same as fig. A.5 but for hot stars.